Resonances in $\bar{p}p \to \omega\eta\pi^0$ in the mass range 1960 to 2410 MeV

A.V. Anisovich [c], C.A. Baker [a], C.J. Batty [a], D.V. Bugg [b], V.A. Nikonov [c], A.V. Sarantsev [c], V.V. Sarantsev [c], B.S. Zou [b,1]

[a] *Rutherford Appleton Laboratory, Chilton, Didcot OX11 0QX, UK*

[b] *Queen Mary and Westfield College, London E1 4NS, UK*

[c] *PNPI, Gatchina, St. Petersburg district, Russia 188350*

Abstract

Data on $\bar{p}p \to \omega\eta\pi^0$ from the Crystal Barrel experiment are presented in the range of beam momenta 600 to 1940 MeV/c. A combined partial wave analysis of these data together with data on $\omega\pi^0$ is reported. The $\omega\eta\pi^0$ data require the presence of a $J^{PC} = 3^{--}$ state with mass $M = 2265 \pm 20$ MeV and width $\Gamma = 170 \pm 35$ MeV and a $J^{PC} = 2^{--}$ state with $M = 2240 \pm 55$ MeV, $\Gamma = 330 \pm 60$ MeV. They also require a 1^{+-} state with $M = 2220 \pm 55$ MeV, $\Gamma = 300 \pm 65$ MeV. In the $\omega\eta$ mass spectrum, the $\omega'(1650)$ is observed with $M = 1664 \pm 17$ MeV, $\Gamma = 260 \pm 40$ MeV.

[1] Now at the Institute of High Energy Physics, Beijing 100039, China

The channel $\bar{p}p \to \omega\eta\pi^0$ is studied in a search for s-channel resonances with isospin $I = 1$ and charge conjugation $C = -1$. These data complement those [1] on the final state $\omega\pi^0$, which also has $I = 1$, $C = -1$. Data are obtained by the Crystal Barrel collaboration in a study of the 7γ final state, where $\omega \to \pi^0\gamma$ and $\eta \to \gamma\gamma$.

The experiment was carried out at LEAR using $\bar{p}$ beams from 600 to 1940 MeV/c, corresponding to the mass range 1960–2410 MeV in the $\bar{p}p$ system. A detailed technical description of the Crystal Barrel detector has been given by Aker et al. [2]; here, we recapitulate only the features essential for the present measurement.

The incident $\bar{p}$ beam is defined by a coincidence between a proportional chamber and a silicon counter of 5 mm diameter, situated ~ 5 cm upstream of the liquid hydrogen target, which is 4.4 cm long. Two veto counters cover the beam ~ 20 cm downstream of the target and define an interaction at the first level of the trigger logic. Charged particle detectors (silicon vertex detector, multiwire chamber and jet drift chamber) surround the target over 98% of the solid angle; they are used as on-line vetos, to provide a second-level trigger for neutral final states. They are also used in the data processing to eliminate the few surviving events containing charged particles.

The γ detection is provided by a barrel of 1380 CsI crystals 16 radiation lengths long, and having an angular resolution of 20 mrad in both polar and azimuthal angles. The γ detection is efficient down to energies of 20 MeV. This is important in the present measurement, since some photons from $\omega \to \pi^0\gamma$ have very low laboratory energies. The energy resolution is given by $\Delta E/E = 2.5\%/E^{1/4}$, with E in GeV. The energy from all CsI crystals is summed on-line, so as to produce a third-level trigger for events having a total energy within 200 MeV of that expected in $\bar{p}p$ interactions [3]. The beam intensity was typically 2×10^5/s and the trigger rate for neutral final states saturated at 60/s.

In the off-line analysis, accepted events are required to contain exactly 7 distinct showers. The reasons for this constraint are as follows. Firstly, photons from high energy π^0 frequently merge into a single shower. However, the resulting events with only six distinct showers are subject to a very large background from the prolific $3\pi^0$ final state. It was found to be impossible to reduce this background to a low level in 6γ events. The second, reverse problem arises when Compton scattering out of a shower generates a low energy photon close to but separate from the primary shower. Such events, containing 8 showers, are too easily confused with $\eta\pi^0\pi^0\pi^0$ events to be useable. The effects of the 7γ selection and further criteria are included in a Monte Carlo simulation using GEANT. In this simulation, events are generated uniformly in $\omega\eta\pi^0$ phase space; after applying experimental cuts, the surviving events simulate the acceptance in the maximum likelihood fit to data.

There is an important point concerning the treatment of the vertex. For events with showers at wide angles from the beam, the vertex may be reconstructed with an accuracy of ~ 1 cm. This is comparable with half the length of the target. However, when events contain several showers close to the beam direction, the reconstruction of the vertex is poorer and events may be reconstructed with vertices well outside the target. We therefore choose to fit the vertex at the centre of the target for all events. The effect on event selection is simulated with the Monte Carlo by generating events uniformly down the length of the target. With the selection criteria we apply in the kinematic fit, the perturbation to acceptance is at most 2% of its magnitude.

Selection of the $\omega\eta\pi^0$ channel and rejection of background depends on the reliability of cuts and the Monte Carlo simulation. Performance checks are most sensitive for 2-body final states, such as $\pi^0\pi^0$, $\pi^0\eta$ and $\eta\eta$. Systematic checks for these channels have been described in earlier publications, e.g. [4]; the treatment of showers and reconstruction efficiencies are identical here.

For present data, the main backgrounds before cuts are from $\omega\pi^0\pi^0$ and from $\eta\pi^0\pi^0\pi^0$ after the loss of one photon. The effects of these and other backgrounds have been studied with the Monte Carlo simulation. After tuning to minimise all backgrounds, the following cuts are selected: (i) Confidence level $CL(\omega\eta\pi^0) > 10\%$, (i) $CL(3\pi^0\gamma) < 0.1\%$, to reject $\omega\pi^0\pi^0$, (iii) $CL(\omega\eta\pi^0) > 0.5 * CL(\pi^0\pi^0\eta\gamma)$, to select well constructed ω; (iv) $CL(\omega\eta\pi^0)$ greater than the confidence level of any other 7γ final state; except for $\omega\pi^0\pi^0$, these other final states have much lower branching ratios than $\omega\eta\pi^0$; (v) to eliminate combinatoric problems where the γ from the decay of the ω is paired with the wrong (spectator) π^0, the best solution is required to have a confidence level at least a factor 5 better than the alternative combination of π^0 and γ. After these cuts, data at 1800 MeV/c, as an example, are subject to a background estimated to be 17.8%. Of this, the largest source is $3\pi^0\eta$ (12.9%). Further small backgrounds arise from $\omega\pi^0\pi^0$ (0.7 %), $4\pi^0$ (0.8%), other channels (2.3%) and wrong pairings of photons in $\omega\eta\pi^0$ (1.1%). These backgrounds are uniformly distributed over the $\omega\eta\pi^0$ Dalitz plots and to a first approximation do not affect the search for resonances, which couple to narrow structures in the Dalitz plots. The $3\pi^0\eta$ background does however create one asymmetry mentioned below. Numbers of events, reconstruction efficiencies and total estimated backgrounds are shown in Table 1.

The quality of results will be illustrated for one beam momentum, 1800 MeV/c. Data are first fitted kinematically to $\pi^0\eta\pi^0\gamma$. This guarantees overall conservation of energy and momentum. Before this fit, the uncertainty in energy for each photon is typically 3%, but after fitting the error falls to $\sim 1.5\%$. Any small errors in energy calibration are greatly reduced at this stage. Fig. 1(a)

Momentum (MeV/c)	CM Energy MeV	Events	ϵ %	total BG %
600	1962	1963	16.4	14
900	2050	10909	15.9	13
1050	2098	4164	15.7	15
1200	2149	14972	15.2	15
1350	2201	9924	15.0	17
1525	2263	7303	14.4	18
1642	2304	8598	14.1	19
1800	2360	9053	13.6	18
1940	2409	10191	13.3	20

Table 1
Numbers of selected events before background subtraction, reconstruction efficiency ϵ, and estimated backgrounds (BG). Column 2 shows the total energy available in the centre of mass system.

shows the resulting mass distribution for $\pi^0\gamma$ pairs near the mass of the ω. There is a clear $\omega(782)$ signal with a mass within 1 MeV of the standard value [5]. This demonstrates that the reconstruction energy is assessed correctly. The mass resolution has a standard deviation of 15 MeV, close to the Monte Carlo prediction of 14 MeV.

Background from the $3\pi^0\eta$ channel has one noticeable effect illustrated in Fig. 1(b). This figure shows the angular distribution for decay photons from ω decay with respect to the incident $\bar{p}$ direction in the rest frame of the ω. This distribution should be symmetric forward-backward for $\omega\eta\pi^0$ events, by charge conjugation invariance. The Monte Carlo simulation shows that $3\pi^0\eta$ background introduces a significant asymmetry, illustrated by the dashed curve on the figure. The data show a similar peaking towards $\cos\theta_\gamma = -1$; its magnitude is consistent within errors with the estimated background. The $3\pi^0\eta$ channel has been studied in detail [6]. Those events depart from a phase space distribution by only small amounts, because of the large number of combinations. Therefore the $3\pi^0\eta$ distribution is treated as following phase space, except for the effect of the kinematic cuts. The data selection and background have been checked at confidence levels varying from 20 to 5%. After correction for background, the number of accepted events follows the Monte Carlo prediction within 1% over this range.

The normalisation of the cross section is obtained by counting the incident beam and the number of detected events, with the correction of Table 1 for reconstruction efficiency. A rate-dependence is observed for the number of successfully reconstructed events [4]; this is believed to originate from pile-up in the CsI crystals. It is accurately the same for events with 4 to 8γ and is therefore monitored by the dependence of the sum of these events as a function of beam intensity. Errors in normalisation are included in integrated cross sections shown below in Fig. 5. There is a further overall normalisation uncertainty of $\pm 5\%$ from target length, but this has no effect on fitted physics.

We now turn to the partial wave analysis. This fits the full process of production and decay using relativistic tensor expressions for J^P up to 5^-. The cross section is summed over photon polarisations from $\omega \to \pi^0\gamma$ decay. Background is taken from the shape of the Monte Carlo simulation of the competing channels after cuts and is adjusted at each beam momentum to the level of estimated backgrounds. Triplet states may couple to $L = J \pm 1$ in the initial $\bar{p}p$ state (e.g. ${}^3S_1$ and ${}^3D_1$). For a resonance, one expects multiple scattering through the resonance to generate the same phase in both coupled states. In the analysis, this relative phase is therefore set to zero. Table 2 below quotes ratios of coupling constants $r = g_{J+1}/g_{J-1}$ in the $\bar{p}p$ initial state.

The dominant channels are (i) $\bar{p}p \to a_0(980)\omega$, and (ii) $\bar{p}p \to a_2(1320)\omega$. This is illustrated by $\eta\pi^0$ mass projections at all momenta, shown in Fig. 2. In the $\omega\pi^0$ channel, $b_1(1235)$ makes a small contribution, illustrated in Fig. 3. In addition, it is necessary to include a broad component as a physics background to the narrow states across the Dalitz plot. It is parametrised by $\eta\pi$ phase space in low partial waves.

There is a strong $\omega\eta$ peak at 1665 MeV, illustrated at all beam momenta in Fig. 4. It is strong at low momenta, particularly 900 and 1050 MeV/c. This peak cannot be fitted with reflections of other processes, but requires an $\omega\eta$ resonance. For this, we have tried quantum numbers 1^{+-}, 1^{--}, 2^{--} and 3^{--}. The best fit is obtained with 1^{--}. The fitted mass and width $M = 1664 \pm 17$ MeV, $\Gamma = 260 \pm 40$ MeV agree well with PDG averages for $\omega'(1650)$, namely $M = 1649 \pm 24$ MeV, $\Gamma = 220 \pm 35$ MeV; the decay to $\omega\eta$ requires orbital angular momentum $L = 1$. The partial wave analysis gives by far the largest contribution from the initial 1^{+-} $\bar{p}p$ state, i.e. with orbital angular momentum $\ell = 0$ in the production process. Remembering the limited phase space for production of the ω' at low beam momentum, this dominance of $\ell = 0$ is plausible. The preference for 1^{--} has been checked at individual beam momenta; from 900 to 1350 MeV/c, log likelihood is better for 1^{--} than for any other quantum numbers by 100–200 at every momentum.

An alternative fit with $J^{PC} = 1^{+-}$ again requires dominant $\ell = 0$ in the production process. This fit is worse than that with $J^{PC} = 1^{--}$ by ~ 500 in log likelihood, despite the fact that there are now four amplitudes for production with $\ell = 0$: production from initial states ${}^3S_1$ and ${}^3D_1$ and decays with both

$L = 0$ and 2. The fit with $J^{PC} = 2^{--}$ is *a priori* somewhat less likely, since it cannot proceed with $\ell = 0$ in the production process, because $J^{PC} = 2^{+-}$ is forbidden for $\bar{p}p$; the resulting fit is worse in log likelihood by 650 than the fit with $\omega(1660)$. Finally, the possibility 3^{--} requires decays to $\omega\eta$ with $L = 3$; with the limited phase space for these decays, this is intrinsically unlikely; it gives a poor fit with log likelihood worse than 1^{--} by 950.

We now discuss s-channel resonances. From the known meson spectrum, one expects states up to 3^{--} ($^3D_3$) and 3^{+-} ($^1F_3$) around the mass of $f_4(2050)$ ($^3F_4$) and up to 5^{--} ($^3G_5$) and 3^{+-} ($^1F_3$) around 2300 MeV. Here we report a combined analysis of $\omega\eta\pi^0$ data with the $\omega\pi^0$ data of Ref. [1]. The $\omega\pi^0$ data contain larger contributions from high partial waves. The $\omega\eta\pi^0$ data reveal lower partial waves which are either absent in decays to $\omega\pi^0$ or less prominent. The s-channel resonances required by the partial wave analysis are shown in Table 2. The intensities of all partial waves are shown in Figs. 6 and 7 and will now be discussed.

The main difficulty in the analysis lies in separating contributions from different triplet partial waves. We therefore discuss first the simpler singlet states. The upper 3^{+-} state makes quite a large contribution to present data and is clearly visible in Fig. 6(c) in decays to $a_2\omega$; it also makes some contribution to the $\omega'(1650)\pi$ D-wave in Fig. 6(i). The lower $^1F_3$ state makes a smaller contribution, visible in decays to $a_0\omega$ and $b_1\eta$, Figs. 6(e) and (g). This latter state at 2034 MeV makes a particularly strong and well defined contribution to $\omega\pi^0$ data discussed in Ref. [1].

The upper $^1P_1$ state is defined better by the present $\omega\eta\pi^0$ data than by $\omega\pi^0$. If this state is omitted from the fit, log likelihood is worse by 363, a definitive amount. It is clearly visible in decays to $a_2\omega$ and $b_1\eta$ in Figs. 6(a), (b) and (f). The $\pi\eta$ phase space contribution to $^1P_1$, shown in Fig. 6(j), also peaks very close to this mass, and may be fitted by the same resonance; even if this contribution is omitted, the upper $^1P_1$ resonance is still required strongly. The lower $^1P_1$ state is demanded by the strong $\omega_1'(1650)\pi$ signal of Fig. 6(h); it appears also in decays to $a_0(980)\omega$, Fig. 6(d). It also contributes strongly to the $\omega\pi^0$ data of Ref. [1].

For $J^P = 3^{--}$, the combined fit requires a significant ρ_3 resonance at 2013 ± 30 MeV with $\Gamma = 165 \pm 35$ MeV; it is visible in decays to $a_0(980)\omega$ in Fig. 7(f). The mass and width are consistent with the $\rho_3(1981)$ which makes a very large and well defined contribution to data on $\bar{p}p \to \pi^-\pi^+$ [7]. The mass is very well determined there, so in our final fit we fix the mass at the weighted mean with present data, namely 1987 MeV. The width, 170 MeV, is also taken from the weighted mean of the two analyses. This low-lying ρ_3 serves as a useful interferometer, helping to determine partial waves at low momenta with $J^{PC} = 1^{--}$ and 2^{--}.

J^{PC}	Mass M (MeV)	Width Γ (MeV)	ΔS ($\omega\eta\pi^0$)	$r_{\bar{p}p}$
1^{+-}	1960 ± 40	210 ± 80	299	
1^{+-}	2220 ± 55	300 ± 65	363	
3^{+-}	2034 ± 15	107 ± 20	128	
3^{+-}	2245 ± 50	350^{+100}_{-50}	185	
1^{--}	1965 ± 30	165 ± 30	186	0.5 ± 0.6
1^{--}	2115 ± 40	230 ± 50	839	$2.5^{+\infty}_{-1.0}$
1^{--}	2300 ± 75	350^{+100}_{-50}	430	-0.4 ± 0.3
2^{--}	1970 ± 35	170 ± 100	85	
2^{--}	2240 ± 55	330 ± 60	198	
3^{--}	2013 ± 30	165 ± 35	61	(0.006)
3^{--}	2265 ± 20	170 ± 35	456	2.5 ± 1.1
4^{--}	2240 ± 25	190 ± 50	79	
5^{--}	2295 ± 75	250 ± 95	78	(0)

Table 2
Resonances fitted to the data; errors cover the full range of systematic variations observed in a large variety of fits with varying ingredients. Values in parentheses are fixed from data of Ref. [7]. The fourth column gives changes in S = log likelihood when each resonance is removed from the fit to $\omega\eta\pi^0$ and all others are re-optimised. The final column shows the ratio $r_{\bar{p}p}$ of coupling constants g_{J+1}/g_{J-1} for production from initial $\bar{p}p$ triplet states.

At higher masses, the present data definitely require a large contribution from a 3^{--} resonance at 2265 ± 20 MeV. It is observed strongly in decays $^3D_3 \to a_2\omega\ ^7S_3$, as shown in Fig. 7(c). There is also some evidence in $\omega\pi^0$ data of Ref. [1] for this state, but its parameters are determined in the combined fit mostly by the present $\omega\eta\pi^0$ data. In this mass range, both $^3D_3$ and $^3G_3$ $q\bar{q}$ states are expected. However, we are unable to resolve these two states, because of the present weakness of polarisation information.

For $J^{PC} = 1^{--}$, there is evidence from data on $\bar{p}p \to \pi^-\pi^+$ for a ρ_1 at 2000 ± 30 MeV with $\Gamma = 295 \pm 85$ MeV [7]. This state appears strongly in the $\omega\eta\pi^0$ channel in $a_0\omega$, Fig. 7(d), though it could be confused there with a possible threshold effect in $\bar{p}p$. It appears strongly also in $\omega\pi^0$ data. Omitting it from the fit to $\omega\eta\pi^0$, log likelihood changes by 186, so its contribution is definitely required. [Our definition of log likelihood is such that it changes by 0.5 for a one standard deviation change to one parameter]. In the combined fit with $\omega\pi^0$, it optimises at $M = 1965 \pm 30$ MeV with $\Gamma = 165 \pm 30$ MeV. The mass is reasonably consistent with that observed in the $\pi^-\pi^+$ channel; the width is somewhat smaller, but the error in Ref. [7] is large. The $\pi^-\pi^+$ data have the advantage that they extend down to a beam momentum of 360 MeV/c (a mass of 1910 MeV) in steps of ~ 100 MeV/c; $\pi^-\pi^+$ polarisation data are available as well as differential cross sections. The polarisation parameter is phase sensitive and helps greatly in determining the mass of this resonance.

At higher masses, further 1^{--} contributions are definitely required. In the $\pi^-\pi^+$ data, there is tentative evidence for a second 1^{--} state at 2145 ± 50 MeV with $\Gamma = 270 \pm 100$ MeV. A $\rho_1(2150)$ has also been reported by GAMS as a strong signal in a study of $\pi^- p \to \omega\pi^0 n$ [8]. In the $\omega\pi^0$ data of Ref. [1], there is little evidence for it. However, in the present $\omega\eta\pi^0$ data it improves log likelihood by 839, a very large improvement. It contributes the large $^3S_1$ peak in $a_2\omega$ in Fig. 7(a). Because it interferes with $\rho_1(1965)$ in several channels,. its mass and width are somewhat correlated with those of the large $\rho_1(1965)$ signal. The mass optimises at $M = 2115 \pm 40$ MeV and the width at 230 ± 50 MeV.

At the top of the available mass range, a further 1^{--} contribution is required. It improves log likelihoood by a large amount in the fit to $\omega\eta\pi^0$, namely 430. However, it does not appear clearly in the intensities of Fig. 7; it interferes with the lower 1^{--} states and is responsible for pulling down the $^3S_1$ and $^3D_1$ intensities at high masses in Fig. 7(d). In some fits, it optimises at ~ 2260 MeV and in others at ~ 2365 MeV. This suggests the possibility that it is parametrising more than one overlapping resonance. One expects from the quark model both a $^3S_1$ and a $^3D_1$ state in the mass range 2200–2400 MeV. Presently, one can only safely say that a strong contribution is required in the mass range 2225–2375 MeV with a poorly determined width, $\Gamma = 350^{+100}_{-50}$ MeV. Data from a polarised proton target are required to separate $^3D_1$ and $^3S_1$ states reliably.

Finally, we have searched for $^3D_2 \equiv \rho_2$ states, $J^{PC} = 2^{--}$. One expects them in the vicinity of $\rho_3(1987)$ and $\rho_3(2265)$. The upper 2^{--} state is quite strong in both present data and $\omega\pi^0$. It optimises at 2240 ± 55 MeV and with a width $\Gamma = 330 \pm 60$ MeV. It is observed here strongly in decays to $a_2\omega$ $^5S_2$ and $a_0\omega$ $^3D_2$ in Figs. 7(b) and (e). In the present data, there is weak evidence for the lower $^3D_2$ state in decays to $a_0\pi$ in Fig. 7(e); however, there is cross-talk with the stronger 1^{--} amplitude. The evidence for this lower 2^{--} state must presently be regarded as tentative.

The contributions to initial $^3G_4$ and $^3G_5$ partial waves are very small from present data, and have almost no effect on resonance parameters.

In summary, there is a strong $\omega\eta$ signal due to $\omega'(1650)$ with $M = 1664 \pm 17$

MeV, $\Gamma = 260 \pm 40$ MeV. There is strong evidence in the $\omega\eta\pi^0$ data for a 3^{--} state at 2265 MeV. There is also evidence for a ρ_3 consistent with $\rho_3(1987)$ observed in $\bar{p}p \to \pi^-\pi^+$ data and a ρ_1 likewise consistent with the $\rho_1(2000)$ reported there. A further 1^{--} state is definitely required by present data at 2115 MeV; there is evidence for a further 1^{--} contribution in the mass range 2225–2375 MeV, but its mass and width are poorly determined. There is also definite evidence for a 2^{--} state at 2240 MeV. Two 1^{+-} states with masses 1960 and 2220 MeV are required by present data; parameters of 3^{+-} states are consistent with stronger signals fitted to $\omega\pi^0$ data.

1 Acknowledgement

We thank the Crystal Barrel Collaboration for allowing use of the data. We acknowledge financial support from the British Particle Physics and Astronomy Research Council (PPARC). We wish to thank Prof. V. V. Anisovich for helpful discussions. The St. Petersburg group wishes to acknowledge financial support from PPARC and INTAS grant RFBR 95-0267.

References

[1] A. Anisovich et al., *Resonances in $\bar{p}p \to \omega\pi^0$ with masses 1960 to 2410 MeV*, submitted to Phys. Lett. B.

[2] E. Aker et al., Nucl. Instr. A321 (1992) 69.

[3] C.A. Baker, N.P . Hessey, C.N. Pinder and C.J. Batty, Nucl. Instr. A394 (1997) 180.

[4] A.V. Anisovich et al., Nucl. Phys. A 652 (2000) 344.

[5] Particle Data Group (PDG), Euro. Phys. Journ. C15 (2000) 1.

[6] A.V. Anisovich et al., Phys. Lett. B477 (2000) 19.

[7] A.V. Anisovich et al., Phys. Lett. B 491 (2000) 47.

[8] D. Alde et al., Zeit. Phys. C66 (1995) 379.

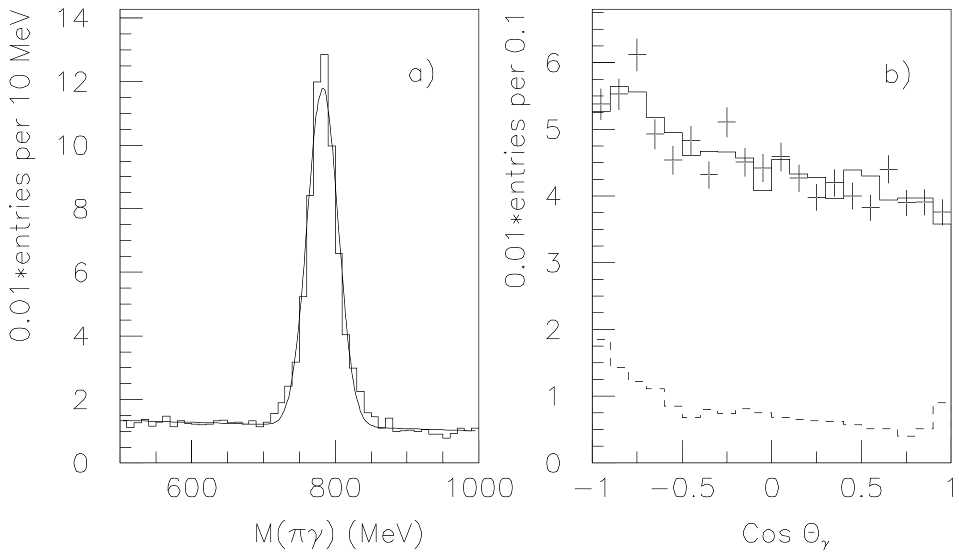

Fig. 1. (a) The mass spectrum of $\pi^0\gamma$ for events fitted kinematically to $\pi^0\eta\pi^0\gamma$; it is fitted with a Gaussian and a linear background; (b) the angular distribution of the γ from ω decay with respect to the beam direction, in the rest frame of the ω; the dashed curve shows the shape of the angular distribution from $3\pi^0\eta$ background; the full line shows the fitted distribution including this background. Data are at 1800 MeV/c.

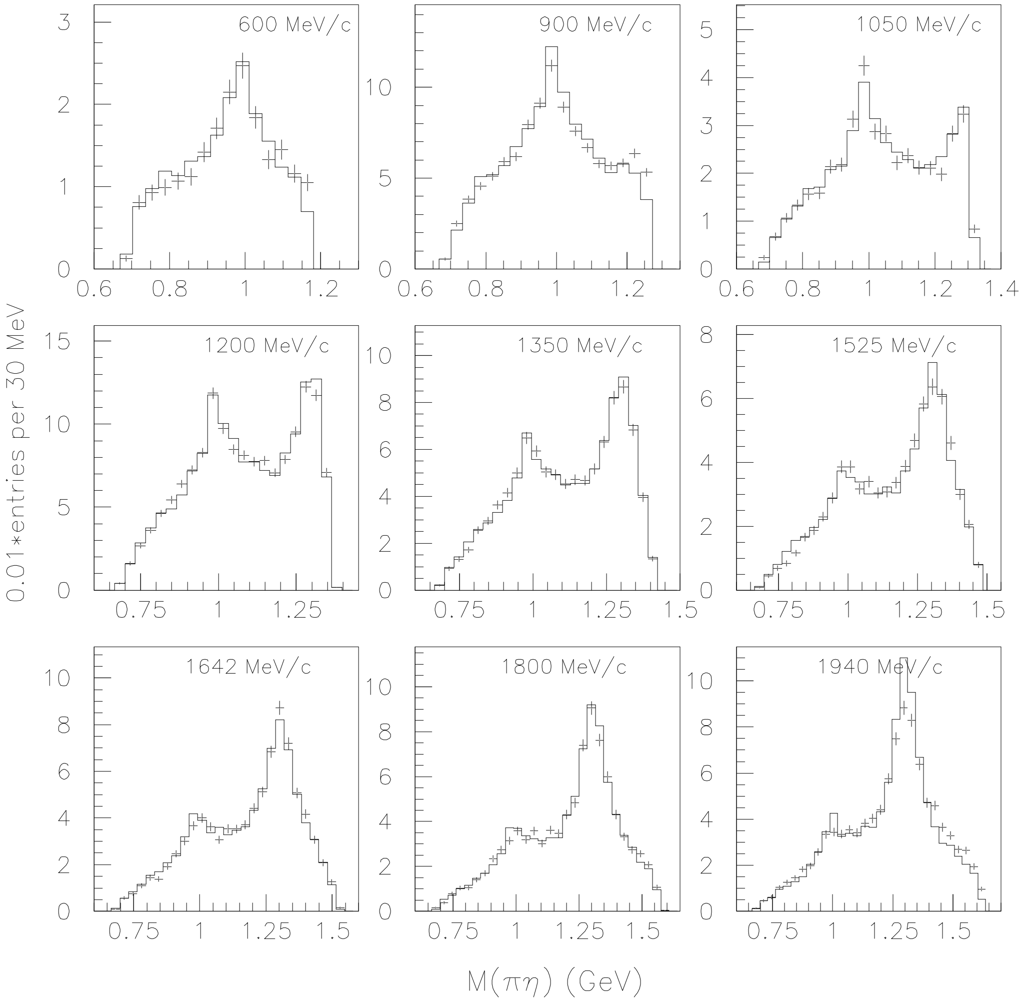

Fig. 2. Projections on to $M(\pi^0\eta)$ at all beam momenta. Full histograms show the result of the partial wave decomposition.

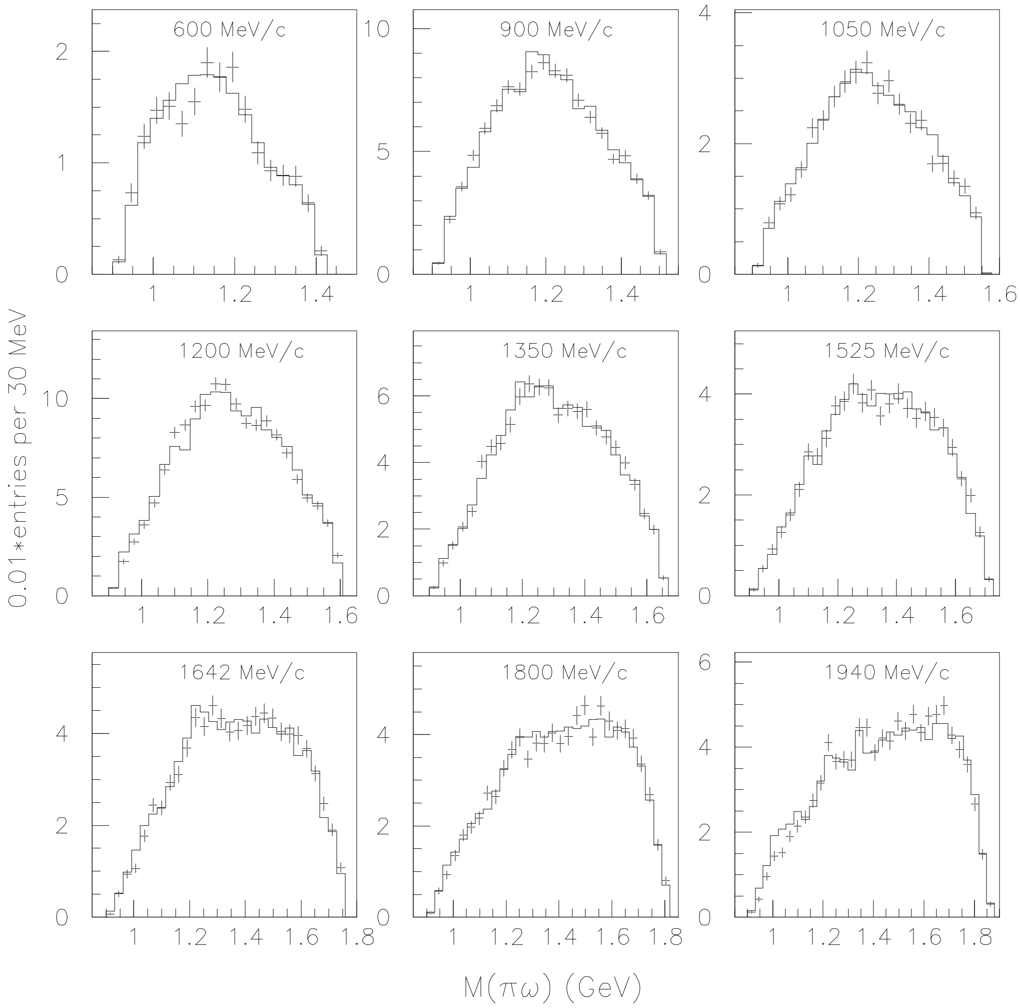

Fig. 3. Projections on to $M(\pi^0\omega)$. Full histograms show the result of the partial wave decomposition.

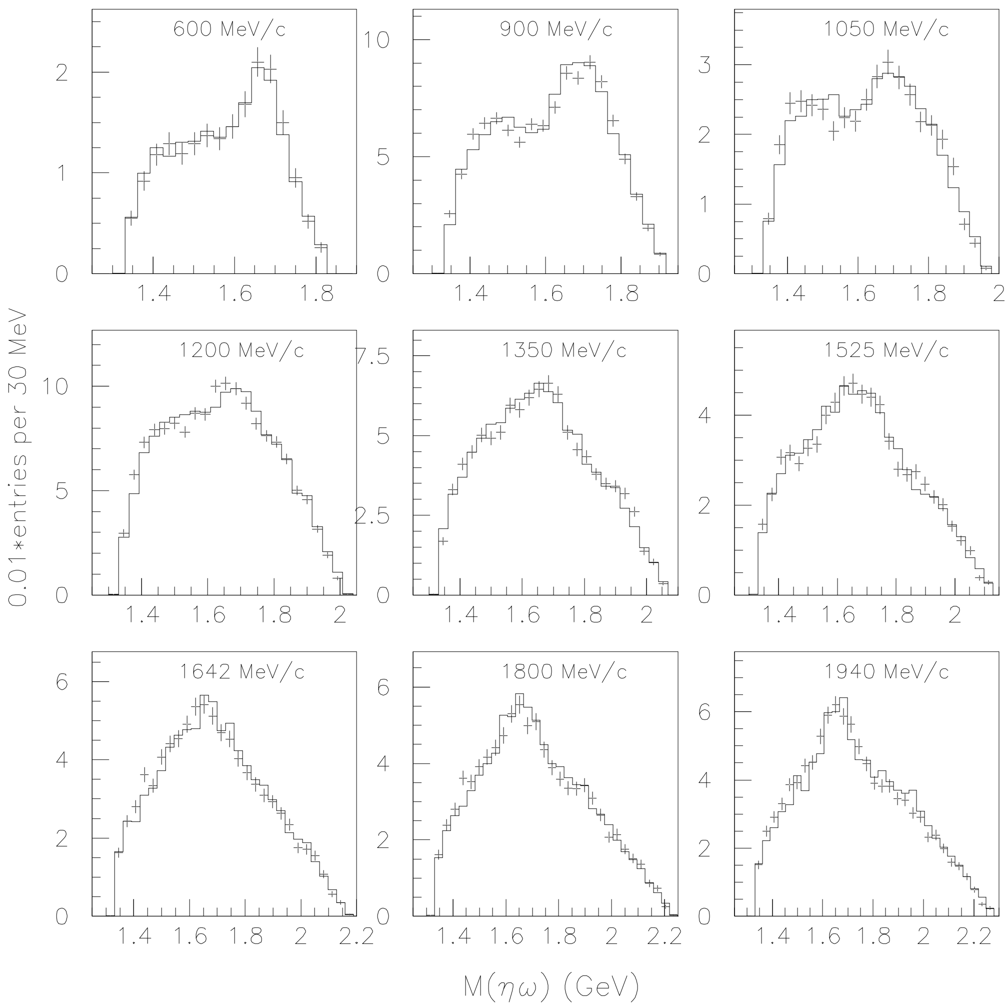

Fig. 4. Projections on to $M(\eta\omega)$. Full histogams show the result of the partial wave fit including an ω' at 1665 MeV with $\Gamma = 260$ MeV.

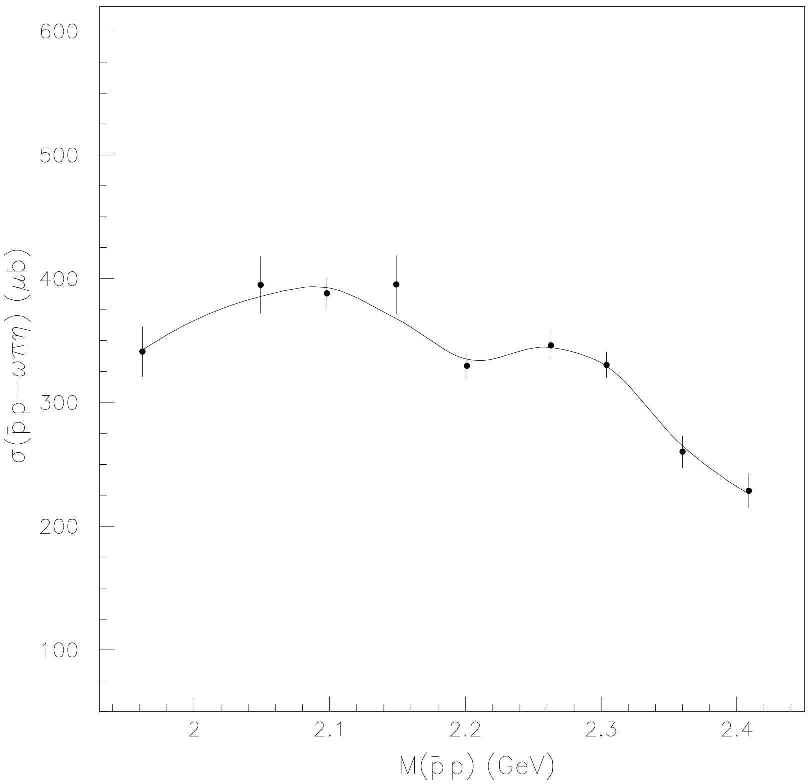

Fig. 5. The integrated $p\bar{p} \to \omega\eta\pi^0$ cross section compared with the fit. It is corrected for acceptance and for branching ratios of the decays $\omega \to \pi^0\gamma$, $\eta \to \gamma\gamma$ and $\pi^0 \to \gamma\gamma$.

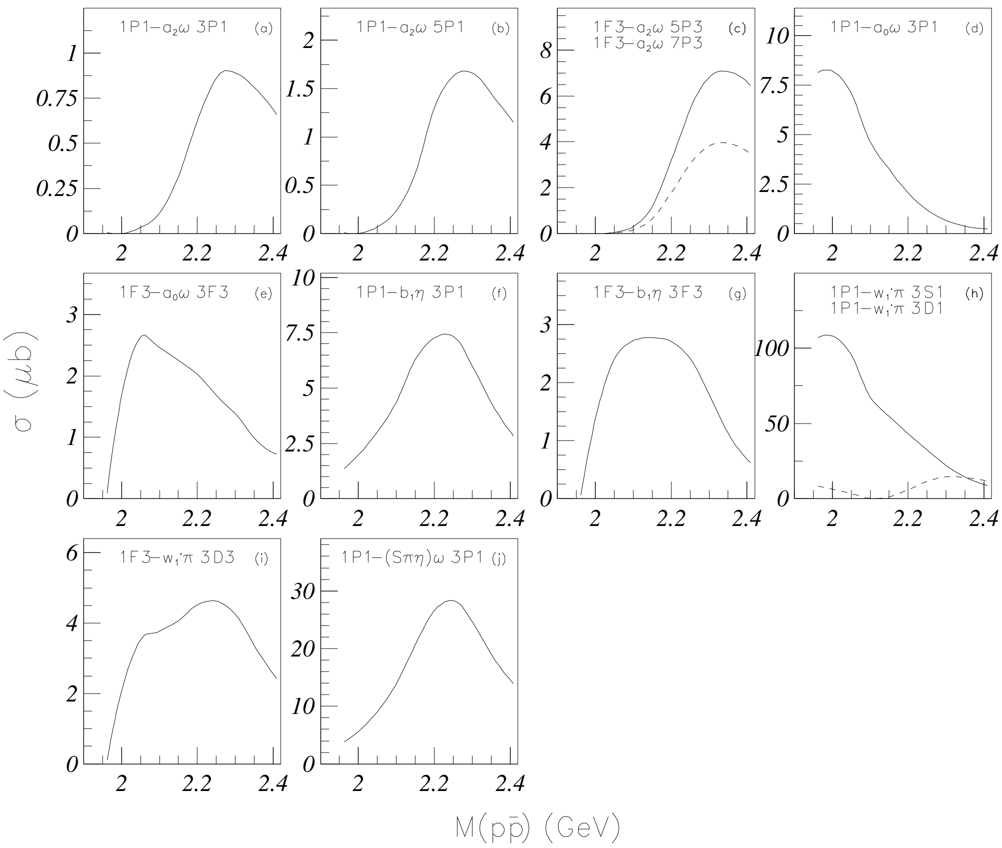

Fig. 6. Intensities of contributions fitted to singlet partial waves. The upper heading on each panel refers to the full curve and the lower one to the dashed curve. $S\pi\eta$ refers to $\pi\eta$ phase space; w_1' refers to $\omega_1(1650)$.

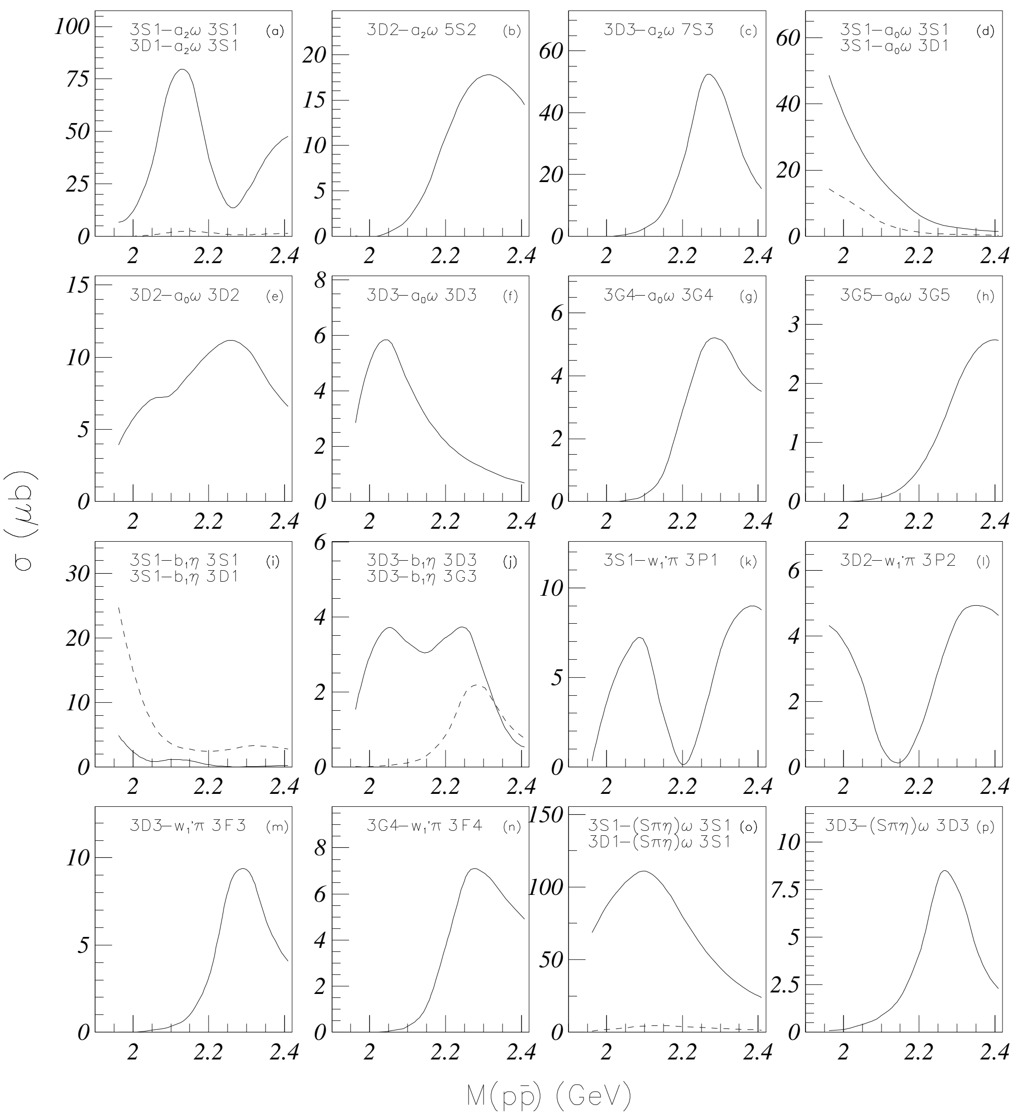

Fig. 7. As Fig. 6 for triplet partial waves.